Tight focusing of axially symmetric polarized vortex beams*

Zhou Zhe-Hai(周哲海)[a)b)†], Guo Yang-Kuan(郭阳宽)[a)b)], and Zhu Lian-Qing(祝连庆)[a)b)]

[a)] *Beijing Key Laboratory for Optoelectronic Measurement Technology, Beijing Information Science and Technology University, Beijing* 100192, *China*
[b)] *Beijing Engineering Research Center of Optoelectronic Information and Instruments, Beijing Information Science and Technology University, Beijing* 100192, *China*

(Received 3 April 2013; revised manuscript received 23 September 2013; published online 10 February 2014)

Tight focusing of axially symmetric polarized vortex beams is studied numerically based on vector diffraction theory. The mathematical expressions for the focused fields are derived. Simulation results show that the focused fields and phase distributions at focus are largely influenced by both the polarization order and topological charge of the incident beams. Moreover, focal spots with flat-topped or tightly-focused patterns can be flexibly achieved by carefully choosing the polarization order and the topological charge, which confirms the potential of such beams in wide applications, such as optical tweezers, laser printing, lithography, and material processing.

Keywords: axially symmetric polarization, vortex beams, tight focusing, beam shaping

PACS: 42.25.Ja, 42.30.Va, 42.62.Be **DOI:** 10.1088/1674-1056/23/4/044201

1. Introduction

Over the past decades, vortex beams have always drawn much attention due to their unique properties and many potential applications.[1–12] The vortex beams possess a helical phase structure of $\exp(\mathrm{i}l\phi)$, where l is the topological charge and ϕ is the azimuthal angle in the cylindrical coordinate system. Because of their dark central core and the ability to transfer angular momentum, vortex beams have been taken into consideration for many applications, such as optical tweezers,[7–9] optical transformations,[10] rotational frequency shifting,[11] and optical vortices.[12] Generally, vortex beams can be generated by computer-generated holograms,[12] programmable liquid crystal displays,[13] and spiral phase elements.[14] Recently, tight focusing of vortex beams with space-variant polarization has attracted the interest of some researchers. Rao *et al.*[15] reported on the focus-shaping technique of cylindrically polarized vortex beams, and showed that the total intensity distribution near focus is dependent not only on the numerical aperture (NA) and the polarization initial angle but also on the topological charge. Pu and Zhang[16] and Zhang *et al.*[17] analyzed the tight focusing of spirally polarized vortex beams, and presented that the intensity distribution and the corresponding orbital angular momentum (OAM) in the focal plane could be moderately controlled, via a reasonable choice of specific spirally polarized state for the incident beams. We also reported on the theoretical and experimental results on tightly focused vector vortex beams.[18] All these reports suggested that the space-variant polarized vortex beams may find wide applications in optical tweezers,[1,2,7–9] laser printing, lithography, and material processing.[1,2]

Recently, a method to generate an arbitrary space-variant vector beam with structured polarization and phase distributions has been presented based on a spatial light modulator (SLM) in a $4f$ system,[19] which will help us to further explore the physics and engineering of vector beams targeting specific applications and to investigate new effects and phenomena of the full vector optical field. To the best of our knowledge, however, the tight focusing properties of such beams have not yet been reported, which has hindered the further applications of such beams. So in this paper, we study the tight focusing properties of axially symmetric polarized vortex beams (ASPVBs), and derive the mathematical expressions for the focused field. Extensive numerical investigations on high-NA focusing of such beams with higher polarization orders are conducted, which indicate that the patterns of the intensity and phase distribution of the focused fields are largely influenced by the topological charge l and the polarization order of the ASPVB.

2. Mathematical expressions

As described in Ref. [19], axially symmetric polarized vortex beams can be expressed as

$$\begin{aligned}\boldsymbol{E}_{\mathrm{in}} = {} & A(r)\exp(\mathrm{i}l\phi)\left\{\cos[(P-1)\phi+\phi_0]\,\boldsymbol{e}_r\right. \\ & \left.+\sin[(P-1)\phi+\phi_0]\,\boldsymbol{e}_\phi\right\}, \end{aligned} \tag{1}$$

where $A(r)$ is the axially symmetric amplitude distribution of the incident beam, P is the polarization order, and l is the topological charge. If $l=0$, the resulting beam is in a purely axially symmetric-polarized beam mode without OAM, which

*Project supported by the National Natural Science Foundation of China (Grant Nos. 61108047 and 61240057), the Program for New Century Excellent Talents in University, China (Grant No. NCET-13-0667), and the Beijing Excellent Talent Training Project, China (Grant No. 2011D005007000008).

†Corresponding author. E-mail: zhouzhehai@bistu.edu.cn

© 2014 Chinese Physical Society and IOP Publishing Ltd

has been discussed in detail in Ref. [20]. Especially if $P=1$, it will be a cylindrically polarized vortex beam, which has been analyzed by Rao *et al.*[15]

In the present paper, the tight focusing of ASPVBs with higher polarization orders is studied. The adopted notation and optical geometry is similar to that of Ref. [21]. Then, the focusing field of an ASPVB can be decomposed into three components, and expressed as

$$\boldsymbol{E}_{\text{out}}(r,\phi,z)=E_r\boldsymbol{e}_r+E_\phi\boldsymbol{e}_\phi+E_z\boldsymbol{e}_z, \tag{2}$$

where $\boldsymbol{e}_r$, $\boldsymbol{e}_\phi$, and $\boldsymbol{e}_z$ are the unit vectors in the radial, azimuthal, and longitudinal directors respectively, and E_r, E_ϕ, and E_z are the amplitudes of the corresponding orthogonal components. Following the theory of Richards and Wolf,[21] the three components at the observation point $S(r_S,\ \phi_S,\ z_S)$ near focus can be expressed as

$$\begin{aligned}\boldsymbol{E}(r_S,\phi_S,z_S) &= \begin{bmatrix}E_r^{(S)}\\ E_\phi^{(S)}\\ E_z^{(S)}\end{bmatrix}\\ &= \frac{-\mathrm{i}A}{\pi}\int_0^\alpha \mathrm{d}\theta\int_0^{2\pi}\exp(\mathrm{i}l\phi)\,l_0(\theta)\sqrt{\cos\theta}\sin\theta\\ &\quad\times\exp\{\mathrm{i}k[z_S\cos\theta-r_S\sin\theta\cos(\phi-\phi_S)]\}\\ &\quad\times\{\cos[(P-1)\phi+\phi_0]\cos\theta\cos(\phi-\phi_s)\\ &\quad-\sin[(P-1)\phi+\phi_0]\sin(\phi-\phi_s)\\ &\quad\cos[(P-1)\phi+\phi_0]\cos\theta\sin(\phi-\phi_s)\\ &\quad+\sin[(P-1)\phi+\phi_0]\cos(\phi-\phi_s)\\ &\quad\times[(P-1)\phi+\phi_0]\sin\theta\}\mathrm{d}\phi,\end{aligned} \tag{3}$$

where $S(r_s,\phi_s,z_s)$ is an observation point near focus, E_r, E_ϕ, and E_z are the amplitudes of the radial, azimuthal, and longitudinal components respectively, A is a constant, $l_0(\theta)$ is the pupil apodization function which denotes the relative amplitude and phase of the incident beam, k is the wavelength number, and θ denotes the focusing angle (the angle between the optical axis and the propagation vector). So the relationship between the maximum of θ and NA of the objective lens is given by $\alpha=\sin^{-1}(NA/n)$, where n is the refractive index of the surrounding medium.

The above field expression can be further simplified using Euler's formula and the identity

$$\int_0^{2\pi}\exp[\mathrm{i}m\phi+\mathrm{i}t\cos(\phi-\gamma)]\mathrm{d}\phi=2\pi\mathrm{i}^m\exp(\mathrm{i}m\gamma)\mathrm{J}_m(t), \tag{4}$$

where m is an integer and $\mathrm{J}_m(t)$ is the Bessel function of the first kind of the order m. Finally, the three orthogonal components of the focusing field can be written respectively as

$$\begin{aligned}&E_r^{(S)}(r_s,\phi_s,z_s)\\ &=\frac{-\mathrm{i}A}{2}\int_0^\alpha l_0(\theta)\sin\theta\sqrt{\cos\theta}\exp(\mathrm{i}kz_s\cos\theta)\\ &\quad\times\{\mathrm{i}^{P+l}\exp[\mathrm{i}(P+l-1)\phi_s+\mathrm{i}\phi_0]\mathrm{J}_{P+l}(X)(\cos\theta+1)\\ &\quad+\mathrm{i}^{l-P}\exp[\mathrm{i}(l-P+1)\phi_s-\mathrm{i}\phi_0]\mathrm{J}_{l-P}(X)(\cos\theta+1)\\ &\quad+\mathrm{i}^{l+P-2}\exp[\mathrm{i}(l+P-1)\phi_s+\mathrm{i}\phi_0]\mathrm{J}_{l+P-2}(X)(\cos\theta-1),\\ &\quad+\mathrm{i}^{l-P+2}\exp[\mathrm{i}(l-P+1)\phi_s-\mathrm{i}\phi_0]\\ &\quad\times\mathrm{J}_{l-P+2}(X)(\cos\theta-1)\}\mathrm{d}\theta,\end{aligned} \tag{5a}$$

$$\begin{aligned}&E_\phi^{(S)}(r_s,\phi_s,z_s)\\ &=\frac{-A}{2}\int_0^\alpha l_0(\theta)\sin\theta\sqrt{\cos\theta}\exp(\mathrm{i}kz_s\cos\theta)\\ &\quad\times\{\mathrm{i}^{P+l}\exp[\mathrm{i}(P+l-1)\phi_s+\mathrm{i}\phi_0]\mathrm{J}_{P+l}(X)(\cos\theta+1)\\ &\quad-\mathrm{i}^{l-P}\exp[\mathrm{i}(l-P+1)\phi_s-\mathrm{i}\phi_0]\mathrm{J}_{l-P}(X)(\cos\theta+1)\\ &\quad+\mathrm{i}^{l+P-2}\exp[\mathrm{i}(l+P-1)\phi_s+\mathrm{i}\phi_0]\mathrm{J}_{l+P-2}(X)(1-\cos\theta)\\ &\quad-\mathrm{i}^{l-P+2}\exp[\mathrm{i}(l-P+1)\phi_s-\mathrm{i}\phi_0]\\ &\quad\times\mathrm{J}_{l-P+2}(X)(1-\cos\theta)\}\mathrm{d}\theta,\end{aligned} \tag{5b}$$

$$\begin{aligned}&E_z(r,\phi,z)\\ &=-\mathrm{i}A\int_0^\alpha l_0(\theta)\sin^2\theta\sqrt{\cos\theta}\exp(\mathrm{i}kz_s\cos\theta)\\ &\quad\times\{\mathrm{i}^{(l+P-1)}\exp[\mathrm{i}(l+P-1)\phi_s+\mathrm{i}\phi_0]\mathrm{J}_{l+P-1}(X)\\ &\quad+\mathrm{i}^{(l-P+1)}\exp[\mathrm{i}(l-P+1)\phi_s-\mathrm{i}\phi_0]\mathrm{J}_{l-P+1}(X)\}\mathrm{d}\theta,\end{aligned} \tag{5c}$$

where $X=-kr_s\sin\theta$. Based on Eqs. 5(a)–5(c), we can separately calculate the intensity distributions corresponding to the three orthogonal components as well as the total field near focus which equals the sum of three orthogonal components.

By analyzing the Bessel functions J_{l-P}, J_{l-P+1}, and J_{l-P+2} in Eqs. 5(a)–5(c), we find that the transverse components of focused fields are not zero on the optical axis on condition that $P=l$ and $P=l+2$, and the longitudinal component also gives rise to a nonzero optical intensity on the optical axis under the condition of $P=l+1$. So the total focused field shows nonzero optical intensity when $P=l$, $P=l+1$, or $P=l+2$.

3. Numerical results

In principle, we can choose any prescribed pupil apodization function $l_0(\theta)$ by using an appropriate pupil filter. Considering that the higher order vector beam can be generated by an interferometric combination of high order Laguerre–Gaussian (LG) beams, an LG beam is used as the pupil apodization function,

$$\begin{aligned}l_0(\theta) &= \exp\left[-\beta^2\left(\frac{\sin\theta}{\sin\alpha}\right)^2\right]\left(\sqrt{2}\beta\frac{\sin\theta}{\sin\alpha}\right)^P\\ &\quad\times\mathrm{L}_l^P\left(2\beta^2\frac{\sin^2\theta}{\sin^2\alpha}\right),\end{aligned} \tag{6}$$

where $\mathrm{L}_l^P(x)$ denotes an associated Laguerre polynomial with radial order l and azimuthal order P. β is the lens filling factor which is the ratio of the pupil radius to the beam waist. In the next simulations, we assume that β=1, $\phi_0=0$, $A=1$, and $n=1$, and all length measurements are in units of wavelength.

3.1. Intensity distributions

First, the intensity distributions at focus (x–y plane) and through focus (z–x plane) on condition that $P = 5$ and $NA = \sin(80^\circ) = 0.985$ are shown in Fig. 1. It can be seen that for the focused beams for $l = 3$, the focused fields each show a wheel pattern, but when $l = 4$ and $l = 5$, the focusing fields each present a tightly focused spot. These phenomena conform to the analysis mentioned above. Moreover, the focal spot size is smallest when $l = 5$, whose full width at half maximum (FWHM) is about 0.55λ, close to the size of the diffraction-limited spot (0.52λ at $NA = 0.985$). Meanwhile, a flat-topped intensity distribution at focus is obtained for $l = 4$, and the focal spot size is about 0.80λ (FWHM). Such a flat-topped focus may find some applications in material processing. Also, it is possible to adjust the focus shape using more complex pupil apodization functions.

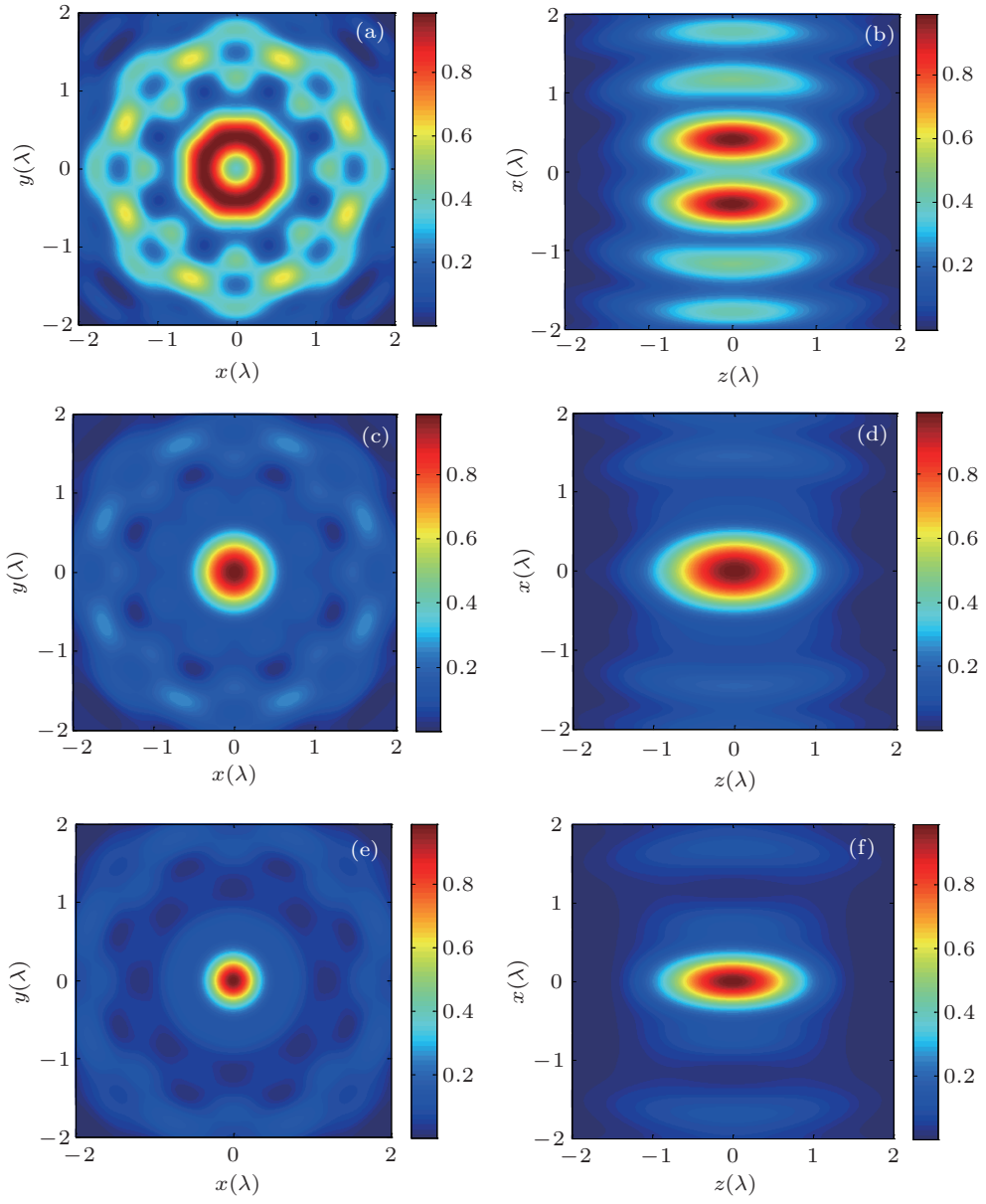


Fig. 1. (color online) Intensity distributions at focus (the left column) and through focus (the right column). (a)–(b) for $l = 3$, (c)–(d) for $l = 4$, (e)–(f) for $l = 5$ respectively.

To further verify our analysis and compare with the results shown in Fig. 1, we also demonstrate the intensity distributions of focused beams for $l = 2$ and $l = 6$, still on condition that $P = 5$ and $NA = 0.985$, which are shown in Fig. 2. Obviously, each of all the focused fields presents a dark-core pattern. For the incident beam with $l = 2$, the focusing field has multiple focusing spots, and the number of spots is related to the polarization order P by $2\times(P-1)$, for example, eight focusing spots for $P = 5$. However, for $l = 6$, the focusing field demonstrates a circular dark-core structure near focus.

For the above shown results, it is safe to say that the specific distribution pattern originates from the spatial interference of the incident beam, which is naturally influenced by the polarization state and phase distribution of the incident beam.

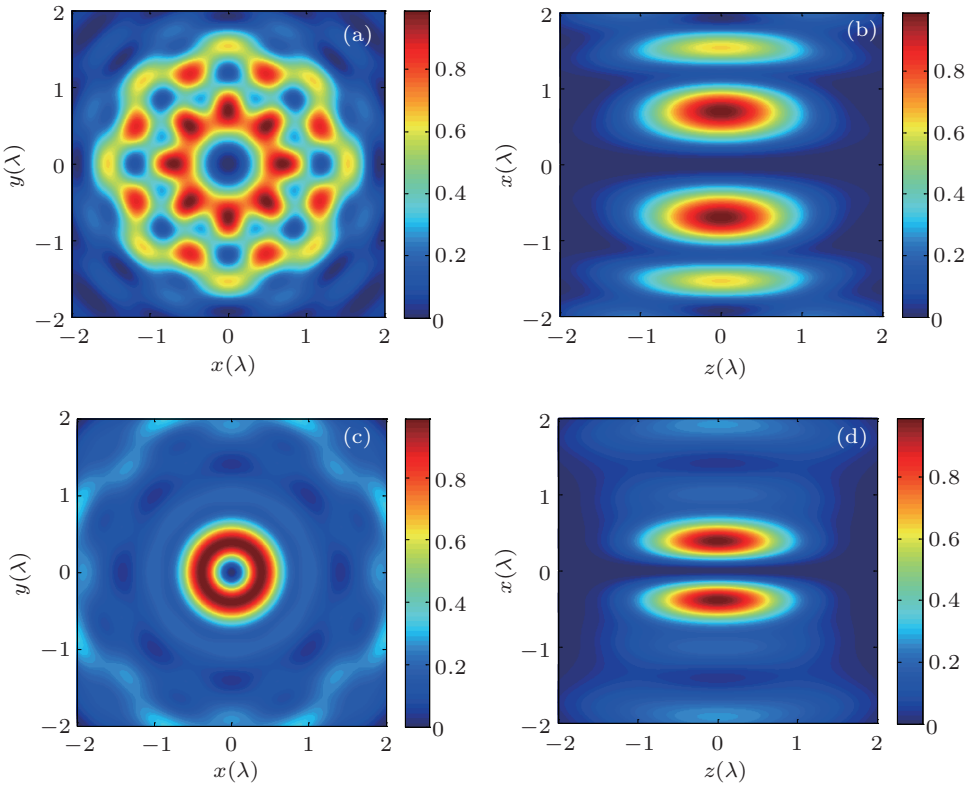


Fig. 2. (color online) Intensity distributions at focus (the left column) and through focus (the right column), and (a)–(b) for $l = 2$, (c)–(d) for $l = 6$, respectively.

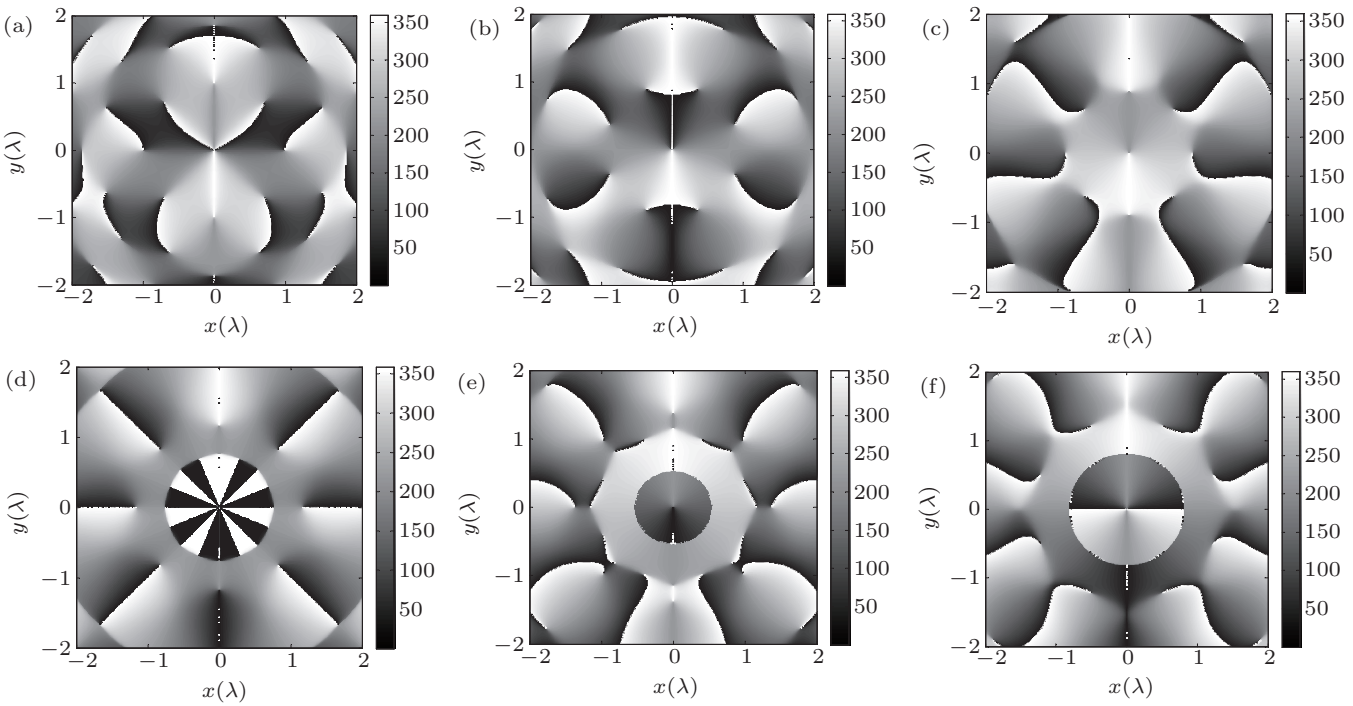


Fig. 3. (color online) Phase contours of the component polarized in the radial direction in the case of $P = 5$: for $l = 1$ (a), 2 (b), 3 (c), 4 (d), 5 (e), and 6 (f). The parameters for calculation are the same as those in Fig. 1.

3.2. Phase distribution at focus

We also calculated the phase distribution of focused field near focus so as to further study the influences of the polarization order and the topological charge on focused fields. The phase contours of the component polarized in the radial direction for different topological charges are given as an example in Fig. 3, and the parameters for calculation are the same as those in Fig. 1. There exists one singularity in the center when $l = 1$, $l = 2$, $l = 6$, and $l = 4$, because of zero axial intensity. The phases near the center for $l = 3$ and $l = 5$ are continuous, which also conforms to the nonzero axial intensity distribution. Moreover, the phase distribution is symmetric with respect to the y axis, and there are multiple singularities around the center. As mentioned above, the complicated phase distribution is related to the intensity distribution, which is dominated by the polarization order and topological charge of the incident beam.

4. Conclusions and discussion

In this paper, we derived the mathematical expressions for the focused field of axially symmetric-polarized beams in a high-*NA* focusing system. The simulation results show that the focusing intensity distribution is influenced by both polarization orders and topological charges of beams. The beams with $P = l$, $P = l+1$, and $P = l+2$ can give rise to nonzero intensity distributions on the optical axis. The focused fields of beams with $P = l+1$ generally present a flat-top pattern, and the intensity distribution near focus for $P = l$ gives rise to the smallest focused spot. The intensity distribution for $P = l+2$ is hollow. Moreover, the phase distributions of different field components are related to their intensity distributions, and a phase singular point occurs at the position where the intensity is zero.

All these irregular phenomena are related to the interference of beams in the high-*NA* focusing system, and the focused field distribution is dominated by the intricate interplay between phase structure and polarization distribution in space. The longitudinal component of the focused field in the high-*NA* system plays an important role in the field distribution. We can manipulate their focusing field distribution of vortex beams by imposing different polarization distributions, which provides a new way to utilize such beams in practice.

Finally, we should note that the focusing field can be tuned more flexibly if we further change the other parameters, such as *NA* of the objective lens, the initial azimuthal angle ϕ_0, and the amplitude distribution of incident beams. ASPVBs may find wide applications such as optical tweezers, laser printing, micro-lithography, and material processing.

References

[1] Soskin M S and Vasnetsov M V 2011 *Prog. Opt.* **42** 219
[2] Vasnetsov M V and Staliunas K 1999 *Optical Vortices* (New York: Nova Science Publishers)
[3] Allen L, Bejiersbergen M W, Spreeuw R J C and Woerdman J P 1992 *Phys. Rev. A* **45** 8185
[4] Allen L and Padgett M J 2000 *Opt. Commun.* **184** 67
[5] Roux F S 2004 *Opt. Commun.* **242** 45
[6] Zhao Y, Edgar J S, Jeffries G D M, McGloin D and Chiu D T 2007 *Phys. Rev. Lett.* **99** 073901
[7] Gahagan K T and Swartzlander G A 1996 *Opt. Lett.* **21** 827
[8] Simpson N B, Dholakia K, Allen L and Padgett M J 1997 *Opt. Lett.* **22** 52
[9] Paterson L, MacDonald M P, Arlt J, Sibbett W, Bryant P E and Dholakia E 2001 *Science* **292** 912
[10] Khonina S N, Kotlyar V V, Shinkaryev M V, Soifer V A and Uspleniev G V 1992 *J. Mod. Opt.* **39** 1147
[11] Courtial J, Robertson D A, Dholakia K, Allen L and Padgett M J 1998 *Phys. Rev. Lett.* **81** 4828
[12] Sacks Z S, Rozas D and Swartzlander G A 1998 *J. Opt. Soc. Am. B* **15** 2226
[13] Wang Q, Sun X W, Shum P and Yin X J 2005 *Opt. Express* **13** 10285
[14] Beijersbergen M W, Coerwinkel R P C, Kristensen M and Woerdman J P 1994 *Opt. Commun.* **112** 321
[15] Rao L Z, Pu J X, Chen Z Y and Yei P 2009 *Opt. Laser Technol.* **41** 241
[16] Pu J X and Zhang Z M 2010 *Opt. Laser Technol.* **42** 186
[17] Zhang Z M, Pu J X and Wang X Q 2008 *Chin. Phys. Lett.* **25** 1664
[18] Zhou Z H, Tan Q F and Jin G F 2011 *Appl. Opt.* **50** G80
[19] Chen H, Hao J, Zhang B, Xu J, Ding J L and Wang H T 2011 *Opt. Lett.* **36** 3179
[20] Zhou Z H, Tan Q F and Jin G F 2009 *Chin. Opt. Lett.* **7** 938
[21] Richards B and Wolf E 1959 *Proc. R. Soc. London Ser. A* **253** 358